Analysis of gravel back-filled borehole heat exchanger in karst fractured limestone aquifer at local scale

Nicola Pastore [a,*], Claudia Cherubini [b,*], Concetta I. Giasi [a]

[a] Polytechnic of Bari, Department of Civil, Environmental and Structural Engineering and Chemistry (DICATECh), via E. Orabona 4, 70125, Bari, Italy
[b] University of Ferrara, Department of Physics and Earth Sciences, via Saragat 1, 44122, Ferrara, Italy

ARTICLE INFO

Keywords:
Borehole heat exchanger
Gravel backfill
Mixed convection
Fractured aquifer
Numerical simulation

ABSTRACT

In designing and sizing of borehole thermal energy system, natural groundwater movement and temperature driven flow have a great importance on the borehole heat exchanger efficiency. The efficiency of double U – tube arrangement in gravel – backfilled borehole installed in a fractured limestone aquifer has been analyzed by means of three – dimensional numerical simulations. The numerical model is representative of 1 m deep of gravel back – filled borehole surrounded by the fractured aquifer. Several simulations have been carried out in order to evaluate the effect of aquifer parameters and boundary conditions on heat exchange efficiency by varying the mean temperature within the double U - tube. The fractured limestone aquifer of the industrial area of Bari (Italy) has been chosen as field site in order to identify the aquifer parameter range and the respective combinations. The results highlight that borehole thermal energy system efficiency is strictly dependent on aquifer transmissivity and groundwater Darcian velocity. The conducted analysis shows that, under lower Darcian groundwater flow and lower aquifer transmissivity, heat transfer efficiency increases at least by 25% compared to stagnant water, whereas heat transfer in the aquifer is governed by heat conduction. The increase of aquifer transmissivity induces the thermosiphon effect enhancing heat transfer processes both in the gravel back-filled borehole and aquifer. At higher values of groundwater Darcian velocity (> 0.1 m/d) advection due to groundwater flow is not negligible and mixed with free convection enhancing heat transfer further. Based on the results, discussion on the performance and environmental constraint of gravel back – filled borehole at field site has been presented.

1. Introduction

The development of cost – effective solutions for district heating and/or cooling systems, combining different renewable integrated energy technologies is a challenge, representing the most effective and efficient solution for the development of modern and sustainable urban and industrial settlements. In this context low enthalpy geothermal system plays a fundamental role, combining and integrating with other renewable technologies in different ways in order to supply the heating and cooling demand of the residential and industrial districts. At least four alternative strategies and combination of them can be implemented in the district heating/cooling system: passive geothermal heating and cooling (Baird, 2013; Zeiler and Boxem, 2009; Ozgener, 2010), seasonal thermal energy storage (Samuel et al., 2013; Xu et al., 2014; Shah et al., 2018; Alva et al., 2018), geothermal heat pump (Trillat-Berdal et al., 2007; Self et al., 2013), geothermal powered absorption chiller (Yilmaz, 2017; Ehyaei et al., 2020).

The present work aims to investigate the potentialities and limitations of the low enthalpy geothermal system on the metropolitan area of Bari (Italy) which presents a great potential to implement renewable heating and cooling integrated systems. In the area groundwater is at lower depth in heterogeneous limestone cretaceous formation offering a great potential for low enthalpy geothermal exploitation.

Borehole Heat Exchangers (BHEs) play a fundamental role in low enthalpy geothermal systems, dissipating or recovering heat from the subsoil and groundwater in order to heat and cool buildings as well as for agricultural and industrial purposes. Geological and hydrogeological conditions determine the efficiency of heat dissipation (recovery) governing the heat transport processes (Williams et al., 2010; Wu et al., 2008; Wagner et al., 2013; Pruess, 2010; Read et al., 2013; Klepikova et al., 2016; Cherubini et al., 2017). Therefore, knowledge of geological settings and understanding of hydrogeological processes is fundamental

* Corresponding authors.
E-mail addresses: nicola.pastore@poliba.it (N. Pastore), claudia.cherubini@unife.it (C. Cherubini).

in order to ensure adequate design and planning of geothermal installations.

Generally, a BHE system is realized in a vertical borehole inside which heat exchangers having different shapes can be installed. A heat carrier fluid, generally water, circulates through the heat exchanger. The borehole volume around the heat exchanger is grout filled with a relatively high thermally conductive material. In presence of an aquifer, groundwater filled borehole or sand/gravel backfilled borehole is commonly used. Under these circumstances, the BHE is permeable and provides a preferential pathway for groundwater exchanging heat with the heat exchanger via natural convection phenomena (Hidalgo et al., 2009). Cross flow mixed convection takes place (Laskowski et al., 2007). Advection due to natural groundwater flow (Banks, 2015) is combined with natural convection due to the difference in groundwater density at various locations (Gehlin et al., 2003). Natural convection is perpendicular to advection increasing the groundwater mixing within the borehole and as a consequence the heat transfer increases.

Installation of groundwater filled BHE in karst fractured limestone aquifers deserves some consideration. Borehole walls could be not stable due to highly fractured zones, empty cavities or filled with residual karstification products. Under these circumstances the installation of a well screen surrounded by a gravel pack is appropriate. In gravel back – filled BHE well screen may not be there, as gravel pack fills uniformly the volume between borehole wall and heat exchanger surface. Then gravel back – filled borehole results more appropriate for such aquifer.

Considering a fractured aquifer with sub horizontal conductive fractures, heated and less dense or cooled and high dense groundwater tends to leave the BHE through the fractures located in upper or lower part of the BHE respectively, with ambient groundwater that tends to enter in the BHE through fractures at larger depth under heat dissipation conditions and through fractures at lower depth under heat recovery conditions (Gehlin et al., 2003; Skarphagen et al., 2019).

Thermal Response Test (TRT) represents a method to evaluate the efficiency of a BHE at a given location by monitoring the effect of short-term heating or cooling and inferring the thermal properties of the ground as well as its hydrogeological conditions (Wagner and Clauser, 2005; Spitler and Gehlin, 2015; Minchio et al., 2020). Anyway, in conventional TRT interpretation BHE is approximated as a line source (Zeng et al., 2002). In presence of groundwater flow, this model has several weaknesses due to the assumptions made on the hydrogeological conditions, BHE arrangement and heat transfer processes that give rise to design errors in low enthalpy geothermal system (Witte, 2013; Poulsen and Alberdi-Pagola, 2015).To overcome these difficulties the moving line source model (Molina-Giraldo et al., 2011) that considers groundwater flow advection can be used. Anyway, both models do not consider free convection processes that take place in the permeable BHE.

TRT interpretation permits to obtain an estimation of the thermal resistance. It represents the key parameters for an optimum design and planning the low enthalpy geothermal system (Luo et al., 2018). In general, thermal resistance represents the ratio of the temperature difference between hot and cold surface to the rate of heat flow per unit area. Then, given the temperature differences between the mean temperature of the heat carrier fluid and the ambient temperature of the ground, the heat transfer rate per unit length of the BHE will be equal to the ratio of this temperature difference and the thermal resistance.

Advection due to the groundwater flow and free convection due to the density driven flow caused by the temperature differences have the effect of reducing the thermal resistance (Gustafsson et al., 2010; Chiasson et al., 2000).

The analysis of the crossed mixed convection in the BHE is still an open issue. In literature, the effect of the advection due to groundwater flow and natural convection due to the changes in water density caused by hot or cold water in the BHE has been addressed separately.

Several authors have studied the effect of the advection due to the groundwater flow on heat transfer processes involving the aquifers and BHE. Claesson and Hellström (2000) and Chiasson et al. (2000) show that advection phenomena by natural groundwater flow do not influence the heat transfer processes with an exception for highly fractured bedrock. Whereas induced groundwater flow by pumping near to the BHE enhanced heat transfer (Gehlin and Hellström, 2003 and Witte, 2001). Banks (2015) investigated advection processes by natural groundwater flow on grout filled BHE. The authors concluded that advection processes become important when Darcian flow is higher than 0.01 md^{-1} and with a Darcian flow higher than 0.1 md^{-1} the effects of groundwater flow are observable in a time frame of less than 3 days. Verdoya and Chiozzi (2015) studied the influence of groundwater flow on the estimation of ground thermal parameters. The authors showed that the infinite line source model is a reliable method to estimate ground thermal parameters if heat transfer phenomenon is dominated by conduction. When the Darcian flow is larger than 0.01 md^{-1} this model fails to estimate the ground thermal conductivity.

Concerning natural convection in a groundwater filled borehole, Keyhani et al. (1983) investigated free convection behavior in vertical annulus with constant heat flux on inner walls and constant temperature at outer wall finding experimental correlation between Nusselt number and Rayleigh number. Gustafsson et al. (2010) conducted three dimensional steady-state simulations using CFD - Fluent estimating a value of borehole thermal resistance in the range 0.07–0.08 mKW^{-1}. Gustafsson and Westerlund (2010) also investigated thermal resistance of groundwater filled borehole by means of TRTs on two BHEs 75 m and 150 m deep. The interpretation of the experimental results shows that thermal borehole resistance decreases from 0.12 mKW^{-1} to 0.065 mKW^{-1} as the injection rate increases in the range of 21–83 Wm^{-1}. Fujii et al. (2009) conducted TRTs using optical fiber sensors in a groundwater filled BHE 30 m deep finding that as heat injection increased in the range of 68–168 Wm^{-1} the thermal resistance decreased from 0.1 to 0.089 mKW^{-1} with a light increase of the thermal conductivity from 2.4 to 2.46 $Wm^{-1}K^{-1}$. Heiko et al. (2012) performed Multi – injection rate TRT in groundwater – filled BHE in hard rock investigating the effect of the forced convection induced by an ordinary pump, showing that the forced convection enhances BHE efficiency, demonstrating that at the same injection rate the required borehole length with forced convection is shorter than without groundwater pumping. Gehlin et al. (2003) investigated the influence of the thermosiphon effect on groundwater filled boreholes in fractured rock, finding that convective flow through the BHE into connecting fractures increases the heat transfer of both borehole and bedrock. Spitler et al. (2016) performed several thermal response tests in a single groundwater filled boreholes 80 m deep with a single U-tube finding an average thermal resistance varying between 0.042 and 0.095 mKW^{-1}.

There are few studies on the gravel back – filled BHE efficiency. Choi and Ooka (2016) investigated the effect of natural convection on thermal response tests conducted in a saturated porous formation comparing gravel backfilled and cement-grouted BHE. The authors affirmed that borehole thermal resistance of the gravel backfilled BHE is lower than cement-grouted BHE.

In the present work a numerical method to investigate the flow and heat transport processes involving the gravel back – filled BHE in fractured karst limestone aquifer is developed investigating the combined effect of advection and natural convection. The developed method represents a framework for estimate the gravel back – filled BHE efficiency.

Computational fluid dynamic (CFD) simulations at local scale are set up on the basis of the boundary conditions and hydrogeologic parameters which refer to the fractured karst limestone aquifer of the Metropolitan area of Bari (Italy). Several numerical simulations have been performed in order to cover the possible hydrogeological conditions of the study area. Thermal resistance of the BHE and groundwater is determined varying the working temperatures, hydrogeological features and boundary conditions investigating the heat transport processes within BHE and groundwater.

Finally, the potential application of the gravel back – filled BHE in the study area are presented and discussed with regards to their

implication on low enthalpy geothermal energy system efficiency and environmental effects.

2. Material and methods

2.1. Study area

The metropolitan area of Bari (Italy) is located in the Apulia Region (South – Eastern Italy), overlooking the Adriatic Sea. The area presents a great potential to implement renewable heating and cooling integrated system since an industrial area with an extension of 1509 ha with more than 800 industries is present with a nearby suburban degraded area devoted to social housing where urban regeneration is needed (district of San Paolo) as well as some significant energy users such as the International Airport and General Hospital (Fig. 1).

Morphologically, the site is characterized by three extended tiered terraces with a height between 40 and 10 m a.s.l. parallel to the coast sloped down to the sea characterized by paleostream channels (lame) perpendicular to the terraces. Stratigraphically, on the Cretacic calcareous dolomitic succession extending in depth even for hundreds of meters (belonging to the known formation of Calcare di Bari) lies transgressively Calcareniti di Gravina formation (lower Pleistocene) with a variable thickness from few meters to 20 m. Alluvial and marshy deposits (Holocene) are detectable at the bottom of lame and some depressions in the dune deposits (Fig. 2).

Groundwater flows in the limestone Cretaceous formation within fractures and karst channels under phreatic or semi-confined conditions mainly in SW-NE direction perpendicular to the coastline, with hydraulic gradients of 0.1–0.5% (Grassi et al., 1986) with a variable depth to water table from about 12–13 m near the coast to 40 m in the most inland zone of the industrial area (Fig. 3). Long term step drawdown tests have been carried out showing a variation of hydraulic transmissivity in the study area in the range 10^{-5} – 10^{-2} $m^2 s^{-1}$ (Cherubini et al., 2018), the rock total porosity presents a value between 1.24%–5.14% (Borgia et al., 2002), whereas the effective porosity assumes a value of about ~0.3% (Masciopinto and Palmiotta, 2016).

The degree of fracturing in the limestone Cretaceous formation is quite variable. Boreholes surveys conducted in the study area highlight the presence of two levels constituted by a carbonate rock sequence intensely fractured and karstified 26 m thick and a lower level

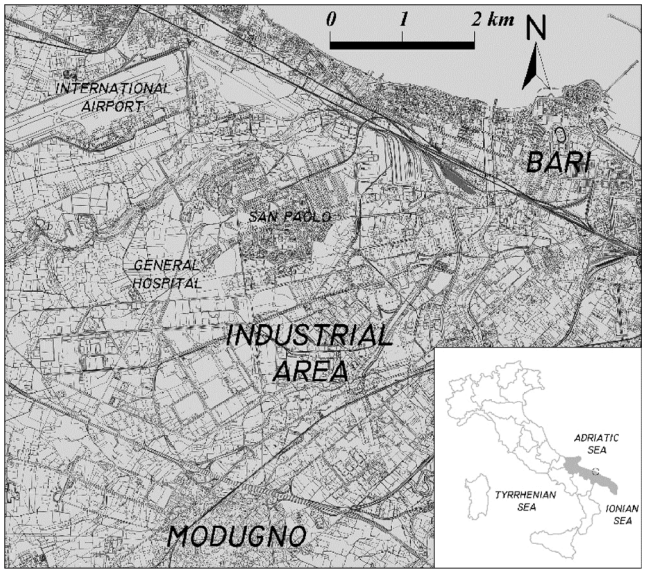

Fig. 1. Industrial area of Bari (Italy) characterized by an extension of 1509 ha with more than 800 industries with the indication of nearby energy users: the district of San Paolo, The International Airport and the General Hospital.

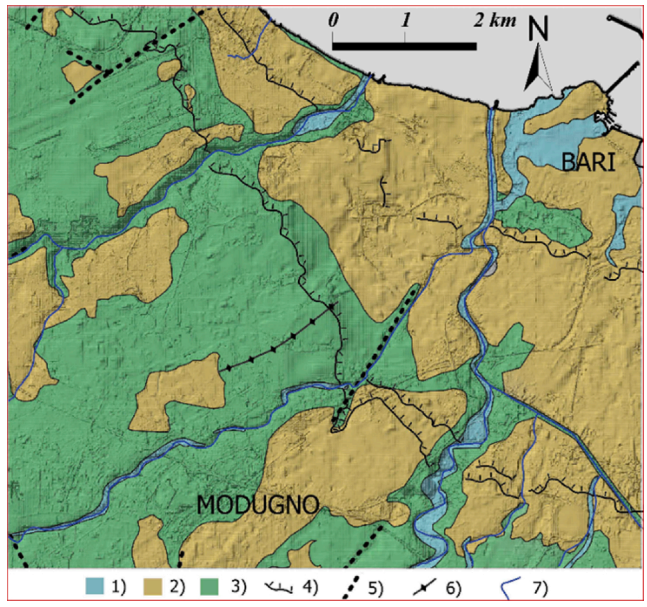

Fig. 2. Geological map of the industrial area of Bari: 1) Alluvial and Marshy deposits (Holocene); 2) Calacareniti di Gravina Formation (Lower Pleistocene); 3) Calcare di Bari formation (Cretaceous); 4) escarpments; 5) Fault (uncertain); 6) Anticlinal axis; 7) Hydrographic network.

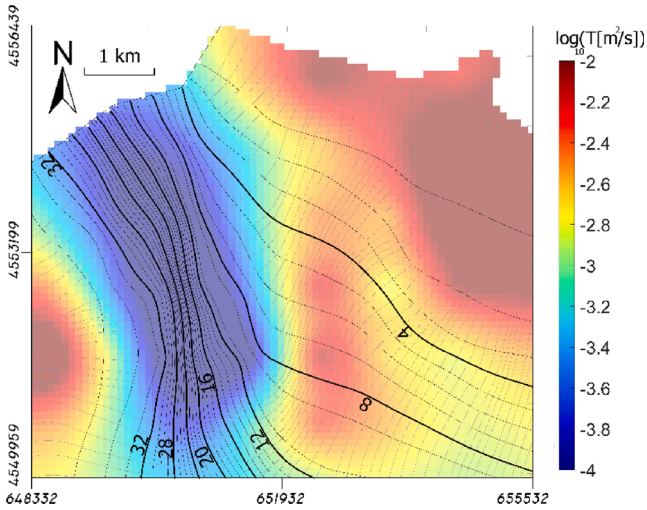

Fig. 3. Contour of groundwater head (m a.s.l.) (black curves), flow paths (gray curves) and hydraulic transmissivity distribution for the study area.

represented by a dolomitic sequence >20 m thick, less fractured and karstified. Billi (2005) investigated the geometrical and structural attributes of fractures and fracture networks of the Apulian Plateau, characterised by a succession of carbonate beds separated by sub – horizontal marked mechanical discontinuities and affected by sub – vertical fractures with bed – parting and bed – unparting behaviour, and by rare faults. The authors found that the fracture spacing is directly correlated to beds thickness variable in the range 0.15–1.20 m.

Di Sipio et al. (2016) investigated thermal properties of the Calcare di Bari formation in dry conditions by means of laboratory tests, finding a value for the thermal conductivity of the limestone between 3.7 and 1.5 $Wm^{-1} K^{-1}$ with a mean value equal to 2.5 $Wm^{-1} K^{-1}$. Typical values of density and heat capacity of limestone are 2700 $kg\,m^{-3}$ and 910 $Jkg^{-1} m^{-3}$ (Robertson, 1988). The mean natural aquifer temperature observed at the site is 290.85 K. Monitoring campaigns in the study area (March – December 2014) showed a diffusive contamination (Cherubini

et al., 2018) especially by chlorinated aliphatic hydrocarbons. Groundwater exploitation for water supply was banned by the public local authority. Thermal anomalies have been detected in correspondence of the hot spot area (Masciopinto and Palmiotta, 2016) which decrease downstream: temperature results higher than the natural aquifer temperature values reaching a value of 292.65 K, suggesting a possible presence of a continuous source of contamination near the hot spot area and possible on going geochemical and biological processes of the organic contaminants in non-aqueous phase.

2.2. Large-scale model

The large-scale model has been used to analyse the hydrogeological features of Bari aquifer. Details on model conceptualization, governing equation, boundary conditions and validation can be found in Cherubini et al. (2018) and Pastore et al. (2020). A brief introduction has been reported for convenience. The fractured and karstic limestone aquifer has been conceptualized by means of the rough walled parallel plate flow model assuming a constant number of independent conductive parallel fracture with spatially variable equivalent aperture. MODFLOW numerical code coupled with inverse numerical approach has been used to model groundwater flow. The two-dimensional domain covers an area of 968.7 km^2 discretised by means of a structured grid of 100 m in size.

The flow model has been validated on the basis of the hydraulic head measurements and point dilution tests. Simulated specific discharge reach the observed specific discharge for a value of conductive parallel of fractures equal to 20. Fig. 4 shows the maps of the space variation of the mean equivalent aperture and flow velocity magnitude with the relative probability density functions. The equivalent apertures present values between $10^{-3.87}$ and $10^{-2.85}$ m following a lognormal distribution. Flow velocity magnitude varies in the range 0.47 - 80.61 md^{-1} with a bimodal probability distribution.

2.3. Local-scale CFD model

A three – dimensional CFD model has been set up in order to analyze the effect of the combination of buoyancy driven flow and natural gradient flow on the BHE efficiency estimating the thermal resistances of the BHE and aquifer.

According to Gustafsson et al. (2010), the numerical model is representative of a section of a 1 m deep of the gravel back-filled borehole surrounded by the fractured aquifer. A double U-tube configuration has been chosen. Fig. 5 shows a sketch of the conceptual model at local scale.

Water with same thermo - physical features circulates in the double U-tube, gravel pack and aquifer. Table 1 shows the water physical parameters as function of the Temperature *T*.

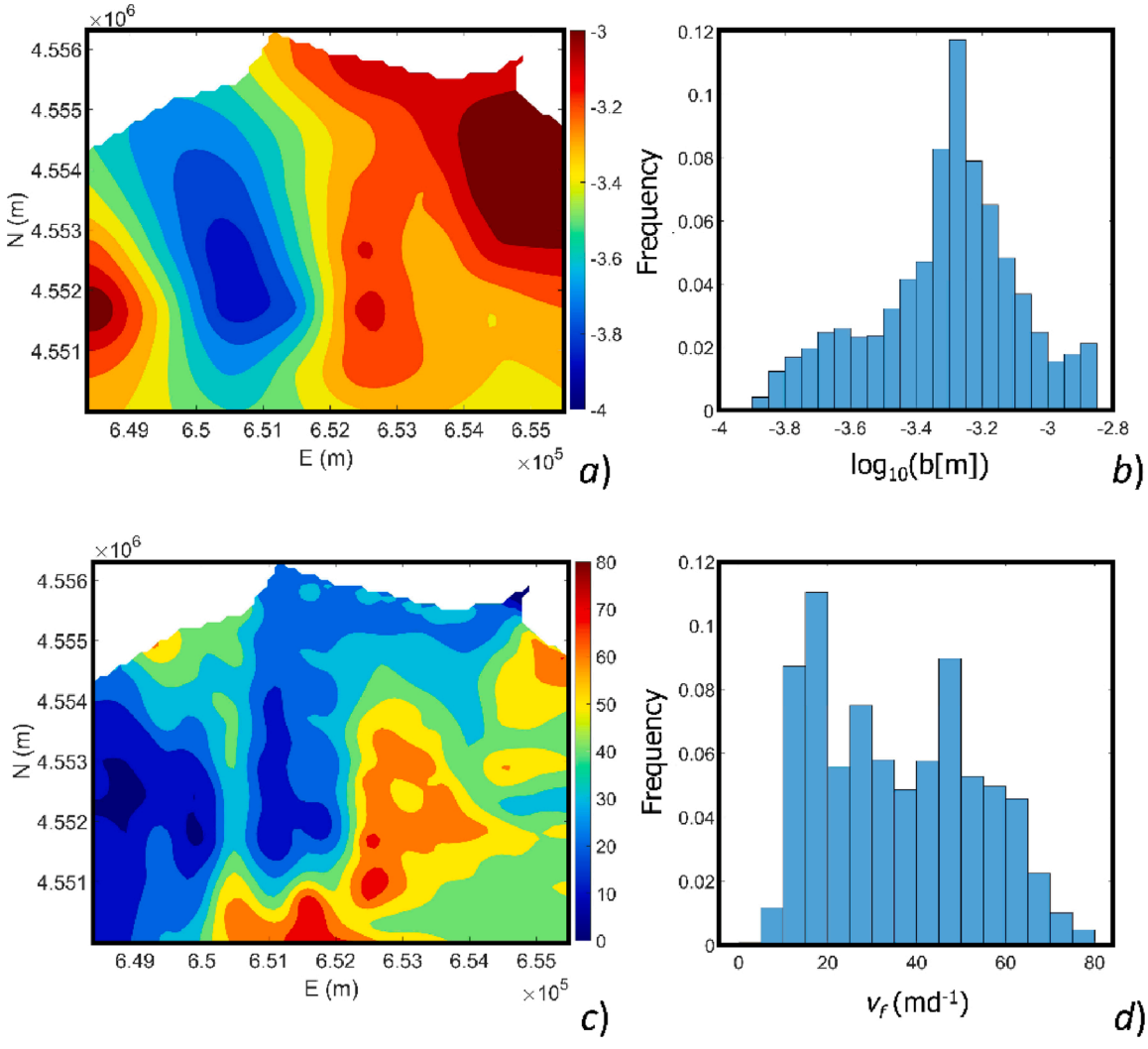

Fig. 4. Mean equivalent aperture and flow velocity magnitude fields for the study area derived by Cherubini et al. (2018) and Pastore et al. (2020) assuming a number of parallel rough walled fractures of 20. *a*) space distribution of the log10 of the equivalent aperture [m]; *b*) probability density function of the log10 of the equivalent aperture [m]; *c*) space distribution of flow velocity magnitude [md^{-1}]; *d*) probability density function of flow velocity magnitude [md^{-1}].

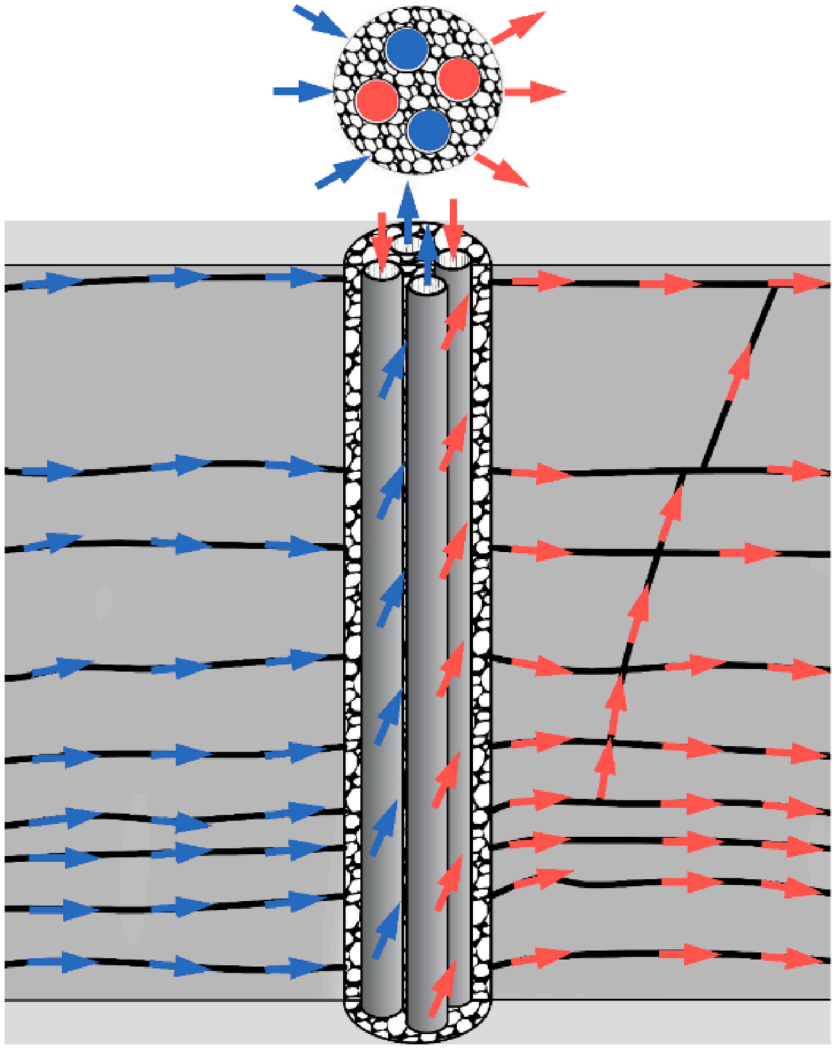

Fig. 5. Sketch of the conceptual model representing a section of 1 m of the gravel backfilled borehole surrounded by the fractured aquifer. The limestone aquifer is conceptualized as a set of sub horizontal conductive fractures. Groundwater flows in the aquifer under natural condition from left to right. Double U-tube heat exchanger heats groundwater in the gravel backfilled borehole. The heated and less dense water tends to leave BHE at the top, whereas groundwater at ambient temperature tends to enter at the bottom. In the BHE natural groundwater flow mixed with free convective flow caused by the density differences between heated water in BHE and groundwater at ambient temperature.

Table 1
Water physical parameter as function of temperature used in the numerical model evaluated using the REFPROP software.

Parameters	Expression
Density ρ_w [kgm^{-3}]	0.0000630927890347^3-0.0603676398828557^2 + 18.9229382407066T+-950.704055329848 (for 273.15< T <293.15) 0.0000103350533197^3-0.0133950656344527^2 + 4.969288832655160T+432.257114008512 (for $T \geq$ 293.15)
Viscosity μ_w [Pa·s]	1.3799566804-0.0212240191517T + 1.3604562827 × 10$^{-4}T^2$+-4.6454090319 × 10$^{-7}T^3$+8.9042735735 × 10$^{-10}T^4$-9.0790692686 × 10^{-13}*T^5+3.8457331488 × 10$^{-16}T^6$
Thermal capacity C_w [J· kg^{-1} K^{-1}]	12010.1471-80.4072879T +0.309866854T^2+-5.38186884 × 10$^{-4}T^3$+3.62536437 × 10$^{-7}T^4$
Thermal conductivity k_w [W· m^{-1} K^{-1}]	−0.869083936 + 0.00894880345T-1.58366345 × 10$^{-5}T^2$ + 7.97543259 × 10$^{-9}T^3$

Local CFD simulations have been conducted in a domain of parallelepiped shape with a size of 4 × 8 × 1 m^3, positioned at depth from $z = -14$ m to $z = -15$ m representing the half of the mean boundary elevation of the shallow aquifer of the field site equal to ~30 m a.s.l. The gravel back – filled BHE is located at coordinates $x = 2$ m and $y = 2$ m presenting a diameter of 0.152 m. Groundwater flow occurs along the x direction. Fig. 6 shows the model conceptualization, the model geometry and the imposed boundary conditions.

In the double U – tube the ratio between the length and diameter is large and the flow inside can be considered fully developed. Water temperature inside the double U – tube has been considered constant for the whole section of the gravel back – filled borehole corresponding to the average value of inlet and outlet temperature. Water circulates inside the U – tubes with a mean velocity u_p [LT^{-1}] and mean temperature T_p [K]. Friction factor f_p [-] can be estimated by means of Churchill equation (Churchill, 1977) for laminar, transitional and turbulent flow:

$$f_p = 8\left[\left(\frac{8}{\mathrm{Re}_p}\right)^{12} + (A+B)^{-1.5}\right]^{1/12} \quad (1)$$

With A and B equal to:

$$A = \left[-2.457\ln\left(\left(\frac{7}{\mathrm{Re}_p}\right)^{0.9} + 0.27\frac{e}{d_i}\right)\right]^{16} \quad (2)$$

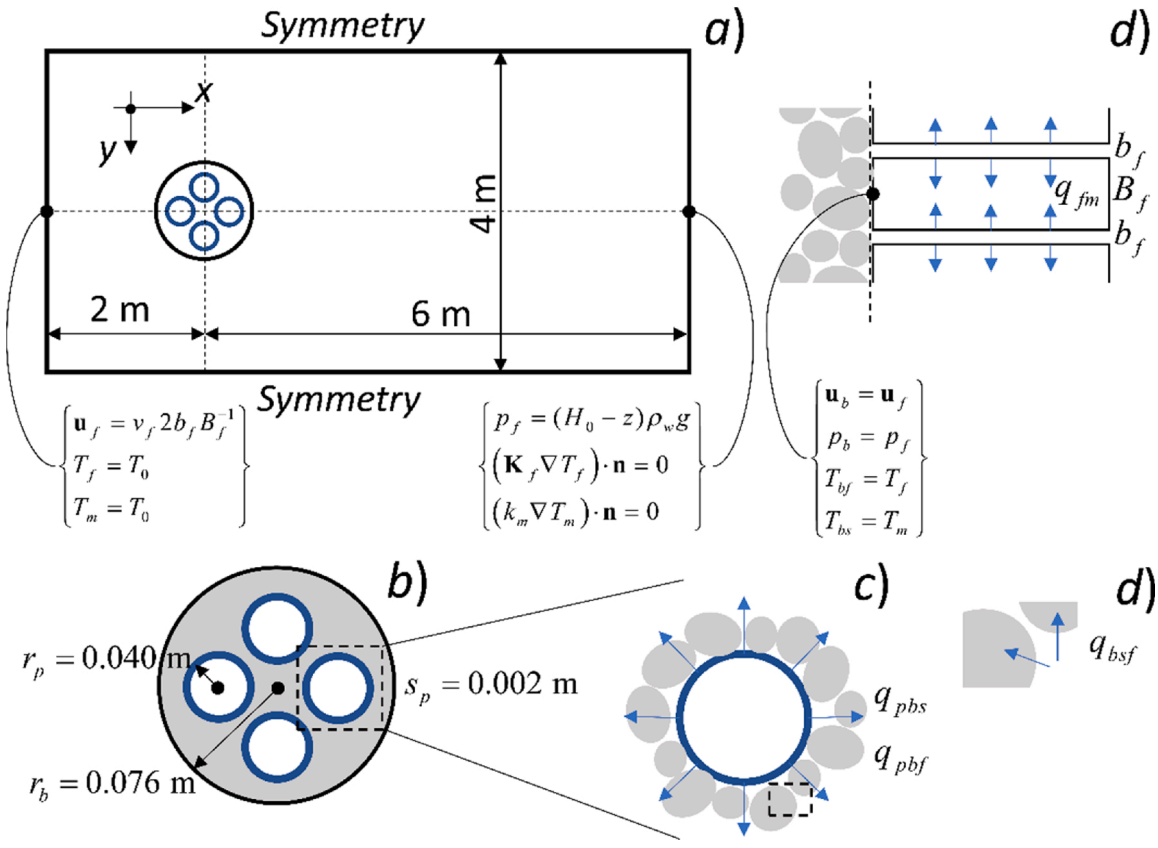

Fig. 6. Model conceptualization, model geometry and imposed boundary conditions. *a*) Plan view of the model domain with imposed boundary conditions: constant flow velocity and constant temperature at upstream face and constant hydraulic head $H_0 = 0$ and no dispersive heat flux at downstream face. Symmetry boundary condition has been imposed to the other faces *b*) gravel back – filled BHE geometry *c*) Heat flow rates between the heat exchanger pipe and both solid and fluid phases *d*) Model geometry of the fractured aquifer with the indication of boundary condition at the interface between the BHE and the fractured aquifer and the heat flow rate between fracture fluid and solid matrix *e*) heat flow rate between fluid and solid phase.

$$B = \left(\frac{37530}{\mathrm{Re}_p}\right)^{16} \tag{3}$$

Where e [L] is the roughness, d_i is the inner pipe diameter and Re_p is the Reynolds number referred to the double U-tube pipe equal to:

$$\mathrm{Re}_p = \frac{\rho_w u_p d_i}{\mu_w} \tag{4}$$

The double U – tube exchanges heat with the borehole according to the temperature differences between the mean temperature T_p inside the pipe and the borehole temperature. The double U – tube exchanges heat in both solid and fluid phase in the borehole according to the following heat transfer rates:

$$q_{pbs} = (1 - \theta_b) h_{ext} (T_{bs} - T_p) \tag{5}$$

$$q_{pbf} = \theta_b h_{ext} (T_{bf} - T_p) \tag{6}$$

Where q_{pbs} [$\mathrm{WL^{-2}}$] and q_{pbf} [$\mathrm{WL^{-2}}$] represent the heat transfer rate between double U – tube and solid and fluid in borehole, respectively. They represent a heat transfer boundary condition between the U-tube and the solid and fluid phase in the boreholes.θ_b [-] is the porosity of the gravel pack, T_{bs} [K] is the borehole temperature of the solid phase, T_{bf} [K] is the borehole temperature of fluid phase. h_{ext} [$\mathrm{WL^{-2}\,K^{-1}}$] is the heat transfer coefficient including internal film resistance and wall resistance of pipe branch composing the double U – tube system expressed by the following equation (Çengel and Boles, 2001):

$$h_{ext} = \frac{1}{\pi d_o} \frac{1}{\frac{1}{\pi d_i h_{\mathrm{int}}} + \ln\left(\frac{d_o}{d_i}\right) k_p^{-1}} \tag{7}$$

Where d_o [L] is the outer pipe diameter, k_p [$\mathrm{WL^{-1}\,K^{-1}}$] is the thermal conductivity of the pipe material with thickness equal to (d_o - d_i)/2 and h_{int} [$\mathrm{WL^{-2}\,K^{-1}}$] is the internal heat transfer coefficient derived by:

$$h_{\mathrm{int}} = \mathrm{Nu}_p \frac{k_w}{d_i} \tag{8}$$

Where Nu_p is the Nusselt number referred to the pipe system representing the ratio between convective and conductive heat transfer phenomena within the pipe. Nusselt number is function of flow regime, for internal laminar forced convection ($\mathrm{Re}_p \leq 3000$) is equal to 3.66, whereas for turbulent forced convection, the Gnielinsky equation (Gnielinski, 1976) is used ($\mathrm{Re}_p > 3000$):

$$Nu_p = \frac{(f_p/8)(\mathrm{Re}_p - 1000)\mathrm{Pr}}{1 + 12.7(f_p/8)^{1/2}(\mathrm{Pr}^{2/3} - 1)} \tag{9}$$

Where Pr is the Prandtl number:

$$\mathrm{Pr} = \frac{C_w \mu_w}{k_w} \tag{10}$$

Flow in borehole considering the thermal expansion of water due to the temperature change, the viscous stress mainly occurring in correspondence of the pipes and the influence of inertia effects is governed by the following mass and momentum conservation laws:

$$\frac{\partial \theta_b \rho_w}{\partial t} + \nabla \cdot (\rho_w \mathbf{u}_b) = 0 \tag{11}$$

$$\frac{\rho_w}{\theta_b}\left(\frac{\partial \mathbf{u}_b}{\partial t} + (\mathbf{u}_b \cdot \nabla)\frac{\mathbf{u}_b}{\theta_b}\right) = -\nabla p_b + \nabla \cdot \left\{\frac{1}{\theta_b}\left[\mu_w\left(\nabla \mathbf{u}_b + (\nabla \mathbf{u}_b)^T\right) - \frac{2}{3}\mu_w(\nabla \cdot \mathbf{u}_b)\mathbf{I}\right]\right\} - \left(\frac{\mu}{k_b} + \rho_w \beta_b |\mathbf{u}_b|\right)\mathbf{u}_b + \rho_w \mathbf{g} \tag{12}$$

Where, k_b [L^2], β_b [L^{-1}] are the permeability and inertia resistance of the packed bed, $\mathbf{u}_b$ [LT^{-1}] is the specific discharge vector, $\mathbf{g}$ [LT^{-2}] is the acceleration gravity vector. Ergun (1953) derived a model to take into account the influence of flow inertia effects correlating permeability and inertia resistance to the porosity and mean particle diameter d_p [L]:

$$k_b = \frac{d_p^2}{150}\frac{\theta_b^3}{(1-\theta_b)^2} \tag{13}$$

$$\beta_b = \frac{1.75}{d_p}\frac{(1-\theta_b)}{\theta_b^3} \tag{14}$$

At each location solid and fluid phase may have different temperatures, therefore each phase needs an energy equation to describe heat transport processes (Pastore et al., 2018):

$$\theta_b \rho_w C_w \frac{\partial T_{bf}}{\partial t} = \nabla \cdot \left[-\mathbf{u}_b \rho_w C_w T_{bf} + \theta_b \mathbf{K}_{bf} \nabla T_{bf}\right] + q_{bsf} \tag{15}$$

$$(1-\theta_b)\rho_{bs} C_{bs} \frac{\partial T_{bs}}{\partial t} = \nabla \cdot [(1-\theta_b) k_{bs} \nabla T_{bs}] - q_{bsf} \tag{16}$$

ρ_{bs} [ML^{-3}], C_{bs} [LT^2K^{-1}] and k_{bs} [$WL^{-1}K^{-1}$] are density and thermal capacitance of packed bed respectively.

$\mathbf{K}_{bf}$ [$Wm^{-1}K^{-1}$] represent the effective thermal conductivity tensor equal to:

$$\mathbf{K}_{bf} = k_w + \rho_w C_w \mathbf{D} \tag{17}$$

Where $\mathbf{D}$ [L^2T^{-1}] is the dispersion tensor as function of the convective velocity $\mathbf{v}_b$=$\mathbf{u}_b$/θ_b, α_L [L] and α_T [L] representing the longitudinal and transverse dispersivity respectively. The components of the dispersion tensor are given by:

$$D_{ij} = \alpha_T |\mathbf{v}_b| \delta_{ij} + (\alpha_L - \alpha_T)\frac{v_i v_j}{|\mathbf{v}_b|}\delta_{ij} = 1 \text{ for } i \neq j \text{ and} \delta_{ij} = 0 \text{ for } i = j \tag{18}$$

Several authors conducted experiments on solute and heat transport in packed beds. On the basis of this result Kambiz (2005) showed a relationship between Peclet number (Pe) and longitudinal and transverse dispersivity from which α_L and α_T result as function of particle diameter as:

$$\begin{aligned} \alpha_L &= 2.8 d_p \\ \alpha_T &= 0.14 d_p \end{aligned} \tag{19}$$

The interaction between fluid and solid phase is represented by the sink – source term q_{bfs} described by the follow equation:

$$q_{bfs} = s_b h_{bfs}(T_{bs} - T_{bf}) \tag{20}$$

Where h_{bfs} [$MT^{-3}K^{-1}$] is the heat transfer coefficient and s_b [L^{-1}] is the specific surface area of gravel packed bed. For spherical grains with constant grain size the specific surface is given by (Kambiz, 2005):

$$s_b = \frac{6(1-\theta_b)}{d_p} \tag{21}$$

In general way the solid to fluid heat transfer coefficient depends on phenomena regarding the convective heat transfer between solid surface and fluid and the internal solid resistance. The Biot number (Bi) represents the ratio between the internal solid thermal resistance and the external thermal resistance due to heat convection. When Bi is much less than unity, the former can be neglected, contrarily for Bi>>1 the latter can be ignored. Stuke (1948) proposed the following model to represent the solid to fluid heat transfer coefficient:

$$h_{bsf}^{-1} = h_{bf}^{-1} + \left(\frac{k_{bs}}{I \cdot d_p}\right)^{-1} \tag{22}$$

Where h_{bf} [$WL^{-2}K^{-1}$] is the solid surface to fluid heat transfer coefficient, I [-] is the dimensionless thermal penetration depth for internal conduction in solid phase equal to $3/2\pi^2$ (Ouyang et al., 2017). h_{bf} is related to the borehole Nusselt number Nu_b as follows:

$$Nu_b = \frac{h_{bf} d_p}{k_w} \tag{23}$$

Handley and Heggs (1968) found that for porous media having spherical particles Nu_b can be estimated as:

$$Nu_b = \frac{0.225}{\theta_b} Re_b^{2/3} Pr^{1/3} \tag{24}$$

Where Re_b is the borehole Reynolds number:

$$Re_b = \frac{\rho_w |\mathbf{u}_b| d_p}{\theta_b \mu_w} \tag{25}$$

The fractured limestone aquifer is conceptualized as a finite number of horizontal rough walled conductive horizontal fractures having both equal mean aperture b_f [L] and fractures spacing $2B_f$ [L]. Flow occurs along the fracture planes along x and y direction governed by the following continuity and momentum equation.

$$\frac{\partial \theta_f \rho_w}{\partial t} + \nabla \cdot (\rho_w \mathbf{u}_f) = 0 \tag{26}$$

$$\frac{\rho_w}{\theta_f}\left(\frac{\partial \mathbf{u}_f}{\partial t} + (\mathbf{u}_f \cdot \nabla)\frac{\mathbf{u}_f}{\theta_f}\right) = -\nabla p_f + \nabla \cdot \left\{\frac{1}{\theta_f}\left[\mu_w\left(\nabla \mathbf{u}_f + (\nabla \mathbf{u}_f)^T\right) - \frac{2}{3}\mu_w(\nabla \cdot \mathbf{u}_f)\mathbf{I}\right]\right\} - \left(\frac{\mu}{k_f}\right)\mathbf{u}_f + \rho_w \mathbf{g} \tag{27}$$

Where θ_f [-] is the effective porosity of fractured aquifer equal to b_f/B_f, p_f [$ML^{-1}T^{-2}$] is the water pressure in the fractures, $\mathbf{u}_f$ [LT^{-1}] is the superficial velocity vector, k_f [L^2] is the permeability of fractured aquifer equal to:

$$k_f = \frac{1}{2B_f}\frac{b_f^3}{12} f_f \frac{Re_f}{96} \tag{28}$$

Where f_f is the friction factor of the fracture which is described by the following equation (Nazridoust et al., 2006):

$$f_f = \frac{123}{Re_f}\left(1 + 0.12\left(Re_f^{0.687}\right)\right) \tag{29}$$

and Re_f represents the Reynolds number evaluated for the fractured media as:

$$Re_f = \frac{\rho_w |\mathbf{u}_f| 2 b_f}{\mu_f \theta_f} \tag{30}$$

In general way, under local non thermal equilibrium condition, heat transport behavior in fractured media can be described using multiple domain concept (Heinze and Hamidi, 2017). Pore fluid, solid matrix and fracture fluid at given location have a different temperature and the interaction between the domains are possible. Anyway, in order to simplify the model, solid matrix and pore fluid are considered in thermal equilibrium. The Limestone of Bari has a relative low matrix porosity equal to ~3%. Then the thermal properties of pore fluid can be neglected. The energy equation for fracture and matrix domain can be

written as follows:

$$\theta_f \rho_w c_w \frac{\partial T_f}{\partial t} = \nabla \cdot \left[-\mathbf{u}_f \rho_w c_w T_f + \theta_f \mathbf{K}_f \nabla T_f \right] + q_{fm} \tag{31}$$

$$\left(1-\theta_f\right) \rho_m c_m \frac{\partial T_m}{\partial t} = \nabla \cdot \left[\left(1-\theta_f\right) k_m \nabla T_m \right] - q_{fm} \tag{32}$$

$\mathbf{K}_f$ [$Wm^{-1}K^{-1}$] represents the effective thermal conductivity tensor for the fracture media, formally equivalent to the $\mathbf{K}_{bf}$ (Eq. 17 and Eq. 18). Dispersion in rough walled fractures can be described as the sum of the contribution of geometrical and Taylor dispersion (Roux et al., 1998). For variable aperture fractures geometrical dispersion assumes a fundamental role reflecting the disorder of the velocity field in the fracture plane. Experimental evidence at field scale shows that dispersion is influenced by large scale preferential flow channels parallel to the mean velocity (Becker and Shapiro, 2000). In hydrogeological systems, dispersion is a scale dependent property (Lallemand-Barres and Peaudecerf, 1978). For this reason, considering an observation scale of 2 m, a value of 0.01 m has been chosen for longitudinal dispersivity according to the scale dependent relationship reported in Beims (1983) with a ratio of 20 between lateral dispersivity and longitudinal dispersivity.

The interaction between fracture fluid and solid matrix is represented by the sink-source term q_{fm} [WL^{-3}] described by the follow equation:

$$q_{fm} = h_{fm} s_f \left(T_m - T_f\right) \tag{33}$$

Where h_{fm} [$WL^{-2}K^{-1}$] is the fracture to matrix heat transfer coefficient in the fracture and s_f (L^2L^{-3}) is the specific surface area defined as the ratio of fracture surface area to the rock volume. For a set of parallel fractures, with uniform fracture spacing equal to B_f and where the porous matrix rock is constituted by prismatic slabs, the specific surface area is equal to $2 \times B_f^{-1}$. For fracture with relatively small aperture Bi is much higher than unity, the heat transfer between fracture and rock matrix is dominated by the solid thermal resistance. Therefore, the thermal resistance between solid surface to fluid can be neglected. Fracture to matrix heat transfer coefficient can be described by the following equation:

$$h_{fm} = \frac{k_m}{I \cdot B_f} \tag{34}$$

For rock matrix blocks having a slab shape, I is equal to $2/\pi^2$ according to Ouyang et al. (2017).

The simulation area has a parallelepiped shape with a size of $4 \times 8 \times 1\ m^3$, positioned at depth from $z = -14$ m to $z = -15$ m representing the half of the mean boundary elevation of the shallow aquifer of the filed site equal to ~30 m a.s.l. The gravel back – filled BHE is located at coordinate $x = 2$ m and $y = 2$ m presenting a diameter of 0.152 m. Groundwater flow occurs along the x direction. Simulations have been performed using COMSOL Multiphysics 4.0a. The built-in modules including the Brinkmann Module, the Heat Transfer in Fluids Module and the Heat Transfer in Solids module have been used in this study. Fig. 6 shows model geometry and imposed boundary conditions. The finite element mesh is composed by 76,290 prisms and 24,000 hexahedra with the minimum element quality equal to 0.2707.

The Double U-tube system is made of HDPE. Each U-tube is characterized by an inner diameter $d_i = 0.04$ m and outer diameter $d_o = 0.044$ m with a thermal conductivity of 0.40 $Wm^{-1}K^{-1}$. Water flows inside each U-tube with a flow rate $Q_p = 5.0333 \times 10^{-4}\ ms^{-1}$ corresponding to a pipe velocity $u_p = 0.40\ ms^{-1}$.

The Gravel pack is supposed to be made from the core drilling material presenting the same thermal parameter of the limestone rock. It is characterized by sub-rounded granules with a diameter $d_p = 9.2 \times 10^{-3}$ m and specific surface $s_b = 348.26\ m^{-1}$ with a porosity $\theta_b = 0.47$.

2.4. Model parameters and key indicators

In order to assess the BHE thermal behavior, borehole thermal resistance R_b [mKW^{-1}], groundwater thermal resistance R_g [mKW^{-1}] and the dimensionless temperature T_D [K] have been chosen as key indicators. They are evaluated as:

$$R_b = \frac{T_{be} - T_{pe}}{\dot{Q}} \tag{35}$$

$$R_g = \frac{T_{be} - T_0}{\dot{Q}} \tag{36}$$

$$T_D = \frac{\left|T_{be} - T_{pe}\right|}{\left|T_0 - T_p\right|} \tag{37}$$

Where $\dot{Q}$ [$m^{-1}W$] is heat flux exchanged per unit length of borehole, T_{pe} [K] and T_{be} [K] are the average temperature at the pipe – borehole interface and borehole – aquifer interface respectively. T_0 [K] is the aquifer reference temperature assumed constant. Note that R_b represents the thermal resistance of the gravel back-filled borehole. The Total resistance of BHE is equal to the sum of R_b and the thermal resistance of the heat exchanger R_p determined as:

$$R_p = \frac{4}{2\pi r_p h_{ext}} \tag{38}$$

Then heat flux is related to temperature gradient between mean temperature pipe T_p and ambient groundwater temperature T_0 as follows:

$$\dot{Q} = \frac{T_p - T_0}{R_p + R_b + R_g} \tag{39}$$

Several transient simulations have been carried with respect to the model outputs $\dot{Q}$, R_b, R_g and T_D to investigate the thermal behavior of the gravel back filled BHE in fractured limestone aquifer varying of the internal mean heat exchanger temperature T_p, and aquifer parameter as: mean fracture velocity v_f [LT^{-1}], mean aperture b_f [L] and number of fracture per meter n_f[L^{-1}].

Groundwater ambient temperature T_0 is set to 291.15 K.

In order to cover all combinations of the possible values of the model parameters, the number of runs needed is $5 \times 5 \times 4 \times 6 = 600$. Each run presents a duration of 72 h imitating a thermal response test procedure.

First, only flow simulations at varying aquifer parameters showed in Table 2 have been carried out with the aim of investigating the relationship between Darcian aquifer velocity $u_f = v_f \times (n_f \times b_f)$ and the averaged Darcian borehole velocity u_{BHE} determined as:

$$u_{BHE} = \frac{\int_V |\mathbf{u}_b| dV}{\int_V dV} \tag{40}$$

With V representing the volume of BHE section. u_f and u_{BHE} showing a linear relationship as:

$$u_{BHE} = \alpha u_f \tag{41}$$

with α equal to 2.8. This factor is representative of the flow field distortion due to the presence of the double U-tube and the gravel pack.

Table 2
Range of model parameter chosen for analysis of gravel backfilled BHE behavior in fractured limestone aquifer.

Parameter	Varied Ranges
v_f [md^{-1}]	0.50; 20.5; 40.5; 60.5; 80.5
$\log_{10}(b_f$ [m])	−2.85; -2.96; -3.12; -3.35; -3.87
n_f [m^{-1}]	1; 2; 3; 7
T_p [K]	278.15; 283.15; 288.15; 293.15; 299.15; 304.15

In order to investigate how much the convective heat flow increases the heat transfer rate compared to the case of only pure thermal conduction, borehole thermal resistance and groundwater thermal resistance have been compared with the relative pure conductive thermal resistance R'_b and R'_g determined via numerical simulation considering only the thermal conduction phenomena. R'_b presents a value between 0.057 – 0.59 mKW^{-1} whereas R'_g is in the range 0.153 – 0.155 mKW^{-1}. The small variations are due to the change of model parameters T_p, n_f and b_f that affect the fluid and thermal conductivities as well as the phase volume fractions of the aquifer. Note that R'_b determined for gravel back – filled borehole has a lower than R'_b determined for groundwater back – filled borehole ranging in the values of 0.113 – 0.118 mKW^{-1}.

According to Spitler et al. (2016), the hydraulic diameter of the borehole section has been chosen as characteristic length to analyse advection and natural convection phenomena in the BHE:

$$D_{BHE} = \frac{\pi r_b^2 - 4\pi r_p^2}{2\pi r_b - 8\pi r_p} \tag{42}$$

Advection regime in the borehole is governed by the Reynolds number Re_{BHE} that can be defined for the borehole section as:

$$Re_{BHE} = \frac{\rho_w (u_{BHE}/\theta_b) D_{BHE}}{\mu_w} \tag{43}$$

The product between Reynolds number and Prandtl number is the Peclet number Pe_{BHE} representing the ratio between advection and conduction phenomena:

$$Pe_{BHE} = Re_{BHE} \times Pr = \frac{u_{BHE}}{\theta_b} D_{BHE} \frac{\rho_w C_w}{k_w} \tag{44}$$

Natural convection regime is governed by the Grashof number Gr_{BHE}

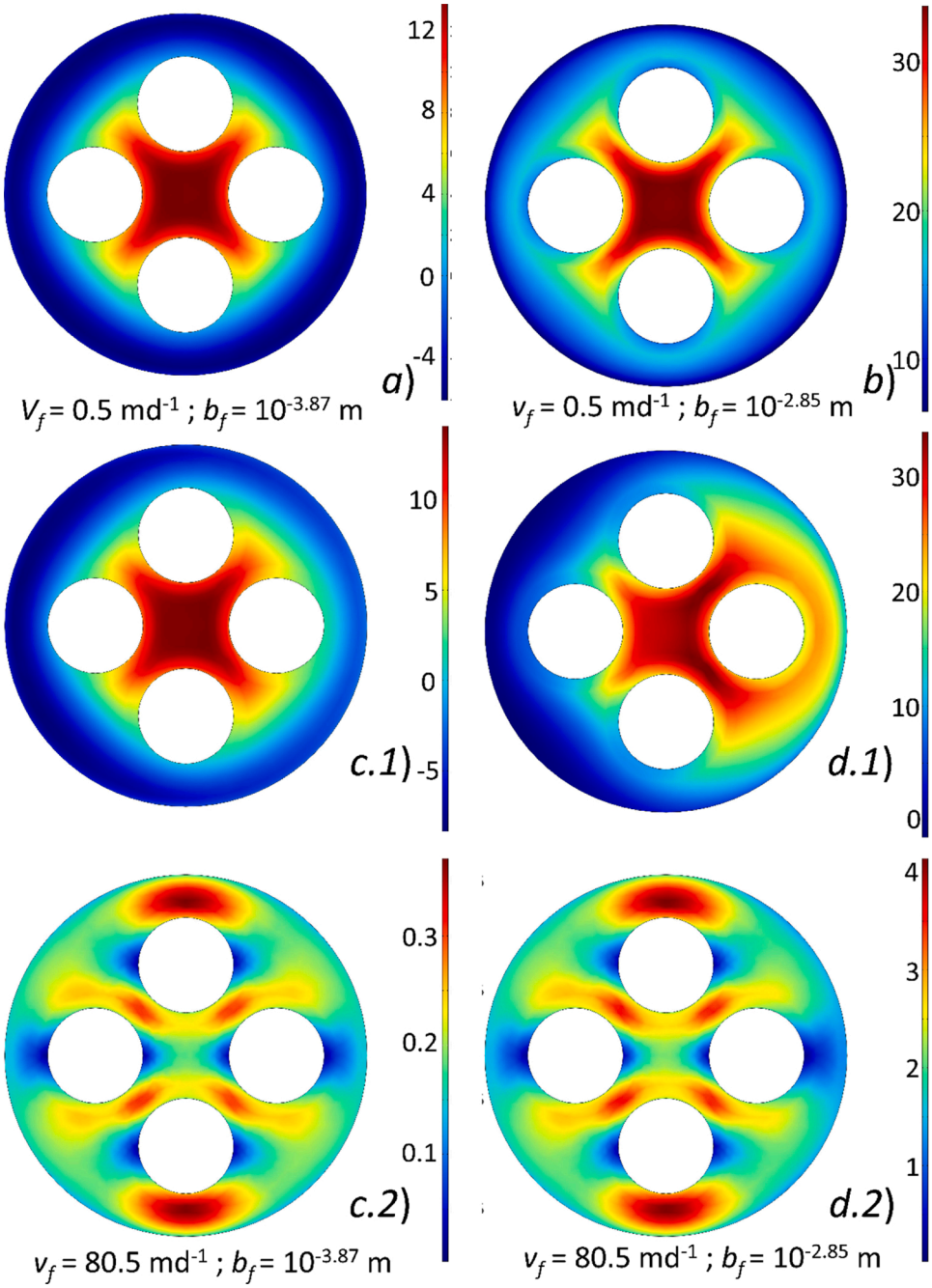

Fig. 7. BHE Darcian velocity distribution expressed in md^{-1} relative to the horizontal section of BHE at z = -14.5 m for T_p =304.15 K and n_f = 7 m^{-1}. a) vertical velocity component for v_f = 0.5 md^{-1} and $b_f = 10^{-3.87}$ m; b) vertical velocity component for v_f = 0.5 md^{-1} and $b_f = 10^{-2.85}$ m; *c.1*) vertical velocity component and *c.2*) horizontal velocity component for v_f = 80.5 md^{-1} and $b_f = 10^{-3.87}$ m; *d.1*) vertical velocity component and *d.2*) horizontal velocity component for v_f = 80.5 md^{-1} and $b_f = 10^{-2.85}$ m.

defined as:

$$Gr_{BHE} = \frac{g\beta_w (T_{pe} - T_{be}) D_{BHE}^3}{(\mu_w/\rho_w)^2} \quad (45)$$

The dimensionless group Gr_{BHE}/Re_{BHE}^2 is the Richardson number Ri_{BHE} representing the relative importance of the natural convection on the advection phenomena.

Borehole heat convective heat transfer can be derived as:

$$h_b = \frac{1}{2\pi r_b R_b} \quad (46)$$

The borehole Nusselt number is given by:

$$Nu_{BHE} = \frac{h_b D_{BHE}}{k_w} \quad (47)$$

3. Results and discussion

Heating or cooling affect the BHE and groundwater flow field changes respect to the model parameters and boundary conditions. Fig. 7 shows the Darcian velocity field[md^{-1}] relative to the *x-y* section of the BHE at z = -14.5 m obtained for T_p =304.15 K, n_f = 7 m^{-1}, minimum and maximum fracture velocity value (v_f = 0.5 md^{-1}; v_f = 80.5 md^{-1}) and minimum and maximum equivalent aperture ($b_f = 10^{-3.87}$ m; $b_f = 10^{-2.85}$ m).

At minimum values of v_f and b_f (Fig. 7*a*) the BHE works as a vertical concentric cylindrical cavity with a hot inner surface and cold outer surface. The contribute of advection is negligible (horizontal velocity components are negligible with respect to vertical ones), natural convection is dominant. The vertical velocity profile is negative at the outer surface and positive at the inner surface. At minimum v_f and maximum b_f (Fig. 7*b*) an ascending flow for the whole BHE section is evident. Advection is still negligible but as the void fraction of the aquifer increases ($n_f \times b_f$), aquifer transmissivity increases, and the aquifer contributes to the natural convection giving rise to a thermosiphon effect. Hot groundwater leaves the BHE in the higher part attracting ambient groundwater from the fractures at lower depth. At maximum v_f and minimum b_f (Fig. 7*c*) the borehole flow field is like case of Fig. 7*a*, but the horizontal flow velocity components are not negligible with vertical velocity distribution characterized by a slight non symmetrical distribution. Due to the low value of void fraction of the aquifer, advection is still negligible. At maximum v_f and maximum b_f (Fig. 7*d*) advection is not negligible having effects on vertical flow distribution showing a nonsymmetrical distribution. Ascending flow is mixed with vertical advection flow.

The dimensionless temperature T_D has been compared with averaged Darcian flow velocity u_{BHE} (Fig. 8). As u_{BHE} increases, T_D presents a constant trend depending on the mean temperature pipe. For T_p values lower than T_0 (Fig. 8*a*), T_D presents a similar constant value equal to ~0.23. For T_p above T_0 (Fig. 8*b*) a significant decrease of T_D at increasingly higher temperatures is evident. At higher T_p water density in BHE becomes lower and buoyancy is higher. Density driven flow enhance heat exchange and T_{be} tends to reach T_{pe}. When u_{BHE} reaches a critical value ~0.3 md^{-1}, T_D increases in an exponential way. In this case, advection is not negligible, mixing with natural convection and T_{be} tends to reach T_0.

Figs. 9 and 10 show the dependencies of the ratios R'_b/R_b and R'_g/R_g varying the mean temperature T_p, Darcian velocities u_{BHE} and $u_f = v_f \times (n_f \times b_f)$ respectively. The equivalent aperture b_f corresponds to the circle size and the number of fractures n_f corresponds to the color scale.

First, let's focus the attention on the values of u_{BHE} lower than ~0.3 md^{-1} corresponding to a value of u_f equal to ~0.1 md^{-1} according to Eq. 41. R'_b/R_b is governed by natural convection reaching the minimum value when b_f is minimal keeping a value slightly higher than unity. Gravel back-filled BHE works as a vertical concentric cylindrical cavity. Advection is negligible and flow recirculates within the BHE governed by the temperature differences between inner and outer surfaces of BHE. For T_p lower than T_0 this lower limit approaches the value of ~1.25. For T_p higher than T_0, the lower limit increases as T_p increases up to a value of ~1.45. R'_g/R_g approaches always the unity and heat transfer is governed by heat conduction phenomena. Then the increase in efficiency ranges from 25 to 45%. Gustafsson et al. (2010) found for water backfilled borehole an efficiency that increases three times compared to stagnant water in the water temperature interval of 283.15–309.15. But R'_b for water backfilled BHE is practically twice the gravel-backfilled borehole.

When b_f and n_f increase, the aquifer void volume increases and as a consequence the aquifer contributes to the natural convection, giving rise to a thermosiphon effect and both R'_b/R_b and R'_g/R_g increase reaching the maximum limit for max values of b_f and n_f. The thermosiphon effect is dependent on the temperature differences between T_p and T_0. The maximum value of R'_b/R_b and R'_g/R_g is obtained for T_p =304.15 K equal to ~3.0 and ~2.6 respectively, with relative increase of efficiency respect to the stagnant water. According to Gehlin et al. (2003) thermosiphon flow enhances the convective heat transfer and can take place if appropriate conditions of b_f and n_f increase aquifer transmissivity surrounding BHE. The enhancement of the BHE efficiency depends on the injected power rate and the transmissivity of the fractures.

For values of u_{BHE} and u_f higher than ~0.3 md^{-1} and ~0.1 md^{-1} respectively, advection is not negligible and contributes to the heat transfer phenomena. Generally, R'_b/R_b and R'_g/R_g increase as u_{BHE} and u_f increase. At lower values of the temperature difference between T_p and T_0 the advection contribution to the heat transfer is more evident,

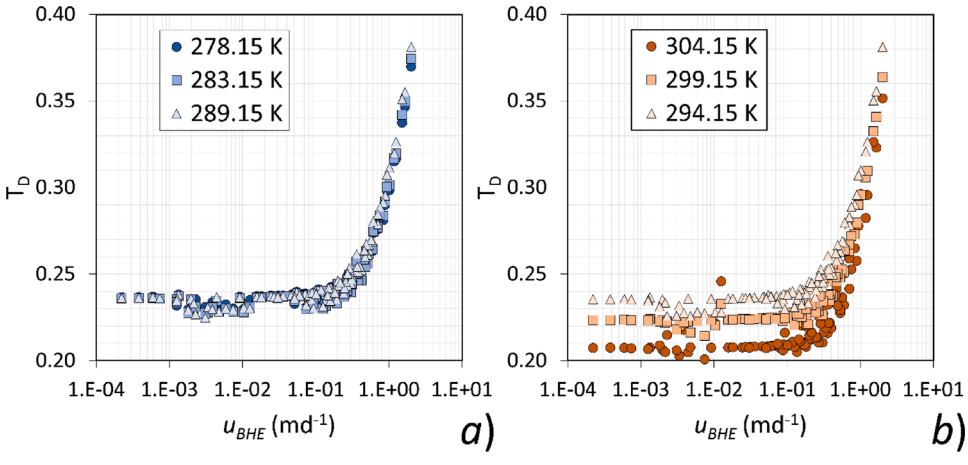

Fig. 8. Dimensionless temperature T_D as function of average darcian velocity u_{BHE}. a) T_p lower than T_0; b) T_p higher than T_0.

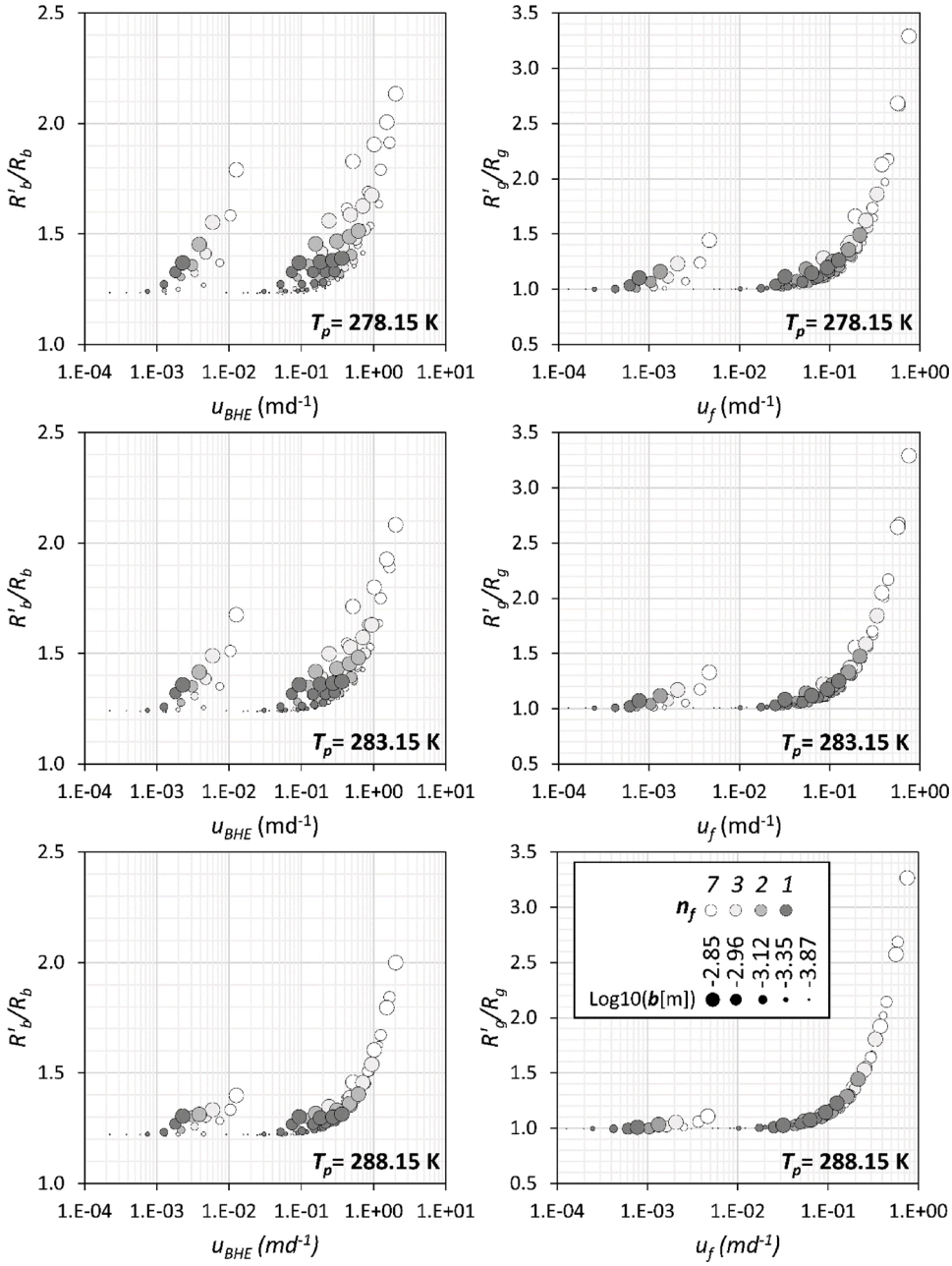

Fig. 9. Thermal resistance ratios R'_b/R_b and R'_g/R_g as function of Darcian velocity u_{BHE} and u_f respectively and for mean temperatures T_p lower than T_0. Equivalent aperture b_f corresponds to the circle size and the number of fractures per meter n_f corresponds to the color scale.

measurable as the differences of the thermal resistance ratio values between the zones with $u_{BHE} < 0.3\ \mathrm{md}^{-1}$ ($u_f < 0.1\ \mathrm{md}^{-1}$) and the zones with $u_{BHE} > 0.3\ \mathrm{md}^{-1}$ ($u_f > 0.1\ \mathrm{md}^{-1}$). When the temperature difference between T_p and T_0 (T_p =288.15 K and T_p =299.15 K) is minimal, the R'_g/R_g values relative to all combination of n_f and b_f follow the same relationship. The contribution of the natural convection is negligible; the aquifer heat transport behavior switches from conductive dominant ($u_f < 0.1\ \mathrm{md}^{-1}$) to advective dominant ($u_f > 0.1\ \mathrm{md}^{-1}$). As the temperature differences between T_p and T_0 increase, natural convection in the aquifer becomes relevant mixing with heat conduction ($u_f < 0.1\ \mathrm{md}^{-1}$) and advection ($u_f > 0.1\ \mathrm{md}^{-1}$) and increasing the heat transfer. According to Banks (2015) the critical value of Darcian velocity of $0.1\ \mathrm{md}^{-1}$ represents the value where the effect of the groundwater flow on the thermal resistance begins to be observed within a time frame of 3 days or less, then groundwater flow effects become observable in TRT test of such duration.

Fig. 11 shows the relationships between $\mathrm{Nu}_{BHE}/\mathrm{Pe}_{BHE}$ and Ri_{BHE} for T_p lower and higher than T_0. Ri_{BHE} assumes very high values indicating that natural convection is the dominating regime inside the BHE. $\mathrm{Nu}_{BHE}/\mathrm{Pe}_{BHE}$ represents the ratio between convection and advection heat transfer rate.

As Ri_{BHE} increases the contribution of convection becomes more relevant dominating the heat transfer phenomena ($Nu_{BHE}/Pe_{BHE} > 1$) within the BHE. $\mathrm{Nu}_{BHE}/\mathrm{Pe}_{BHE} - \mathrm{Ri}_{BHE}$ follows a power law like:

$$\frac{\mathrm{Nu}_{BHE}}{\mathrm{Pe}_{BHE}} = C \times \mathrm{Ri}_{BHE}^{n} \tag{48}$$

With $n = 0.5$ and C depending on T_p and C is variable in the range between 0.0013 and 0.0017 with an average value of 0.0015. The two graphs show a quite similar behavior except that as the temperature difference between T_p and T_0 increases, the buoyancy effect becomes relevant increasing Ri_{BHE} and as consequence the $\mathrm{Nu}_{BHE}/\mathrm{Pe}_{BHE} - \mathrm{Ri}_{BHE}$

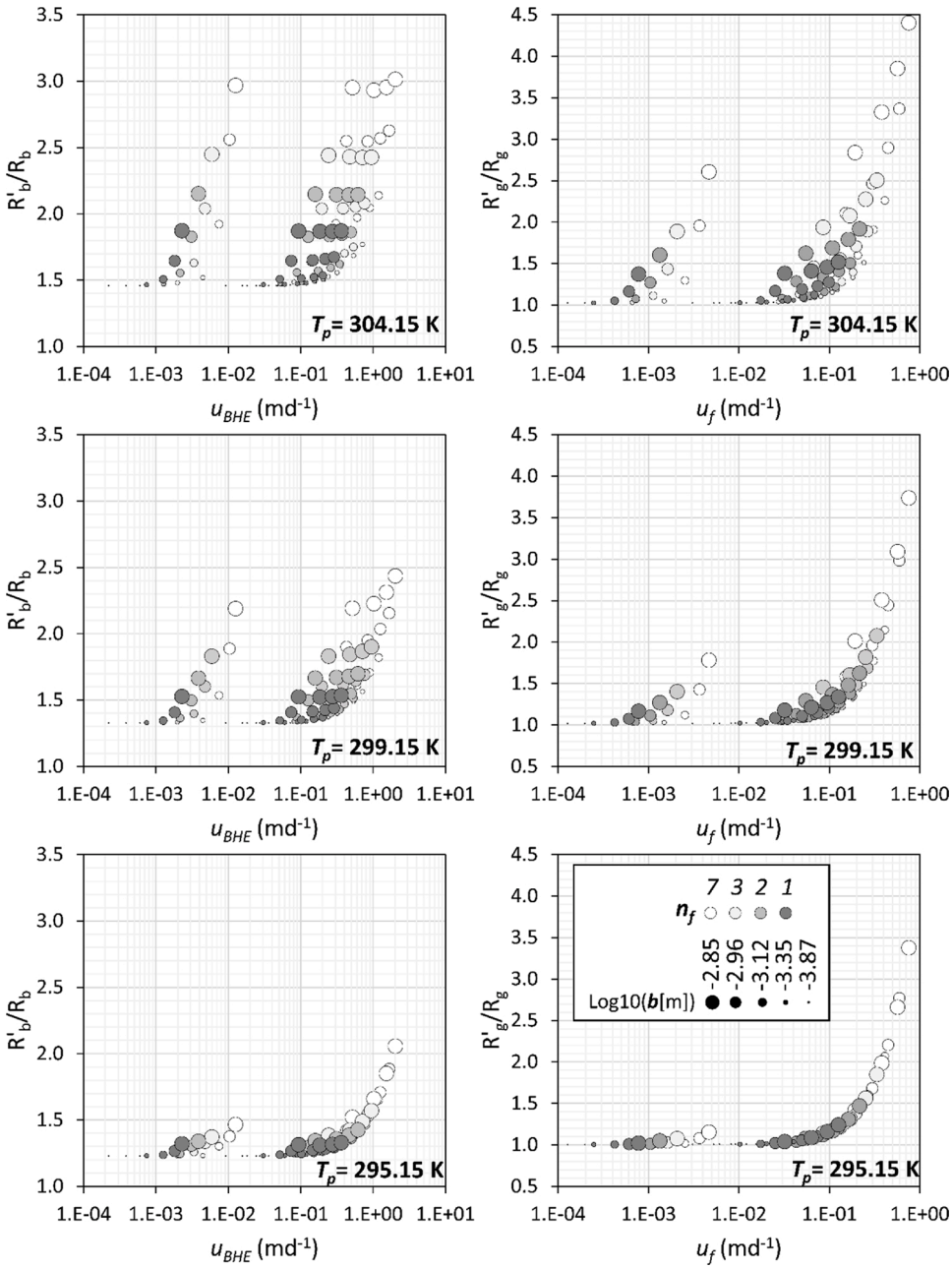

Fig. 10. Thermal resistance ratios R'_b/R_b and R'_g/R_g as function of Darcian velocity u_{BHE} and u_f respectively and for mean temperatures T_p higher than T_0. The equivalent aperture b_f corresponds to the circle size and the number of fractures per meter n_f corresponds to the color scale.

curve moves more to the right. This effect is more evident for values of T_p higher than T_0 due to the greater variation of water density with respect to the temperature.

Once the relationship between the thermal resistance and the model parameters is set up, a map of the average thermal distribution for the field site can be determined. For each couple of v_f and b_f derived by the large scale flow model, R_b and R_g have been determined for varying T_p and n_f. Then, the calculated thermal resistances have been divided in two groups depending on whether the BHE works in heat recovery mode ($T_p < T_0$) or heat dissipation mode ($T_p > T_0$). For each group, the average thermal resistance maps have been obtained by averaging the maps determined for each value of T_p and n_f. (Fig. 12).

The average thermal distributions determined are coherent with the hydrogeological conditions at the field site, decreasing as velocity and equivalent aperture increase reaching minimum values near the coast where the aquifer transmissivity is higher. Gravel back-filled works well in all zones its total thermal resistance varying in the range of $0.045 - 0.055\ \mathrm{mKW^{-1}}$ in heat dissipation mode and in the range of $0.053 - 0.061\ \mathrm{mKW^{-1}}$ in heat recovery mode. Thermal resistance of the gravel back-filled BHE is always lower than the limit of stagnant condition ($R'_b + R_p = 0.073 - 0.069\ \mathrm{mKW^{-1}}$). Gravel back – filled BHE works like a high thermal conductivity grout filled BHE. For instance, for double U- tube grout filled BHE thermal resistance varies in the range $0.109 - 0.054\ \mathrm{mKW^{-1}}$ corresponding to a thermal conductivity of grout material in the range $0.73 - 1.85\ \mathrm{Wm^{-1}\,K^{-1}}$ (Baietto et al., 2010).

Aquifer thermal resistance approaches the pure conductivity thermal resistance ($R'_g = 0.153 - 0.154$) in the upstream zone where aquifer transmissivity is lower.

4. Conclusions

This study assesses the gravel back – filled BHE performance in a

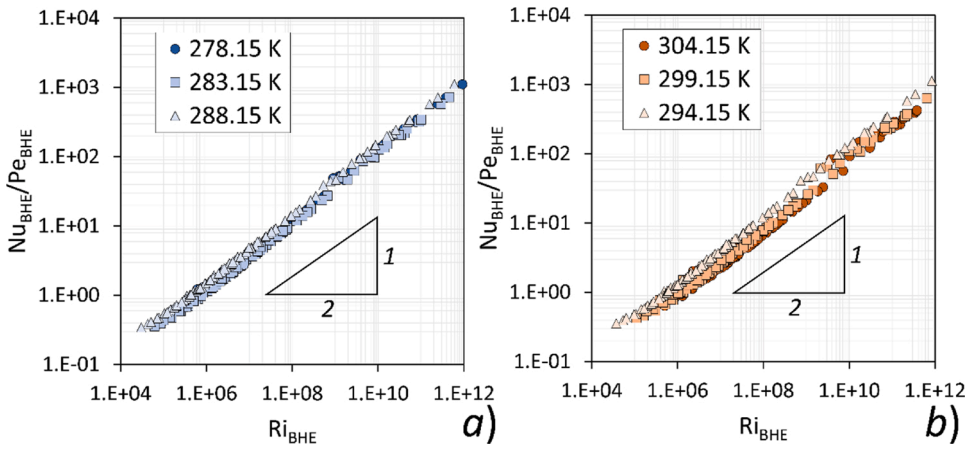

Fig. 11. Ratio between Nusselt number and Peclet number Nu_{BHE}/Pe_{BHE} as function of Richardson number Ri_{BHE} for *a*) T_p lower than T_0 *b*) T_p higher than T_0.

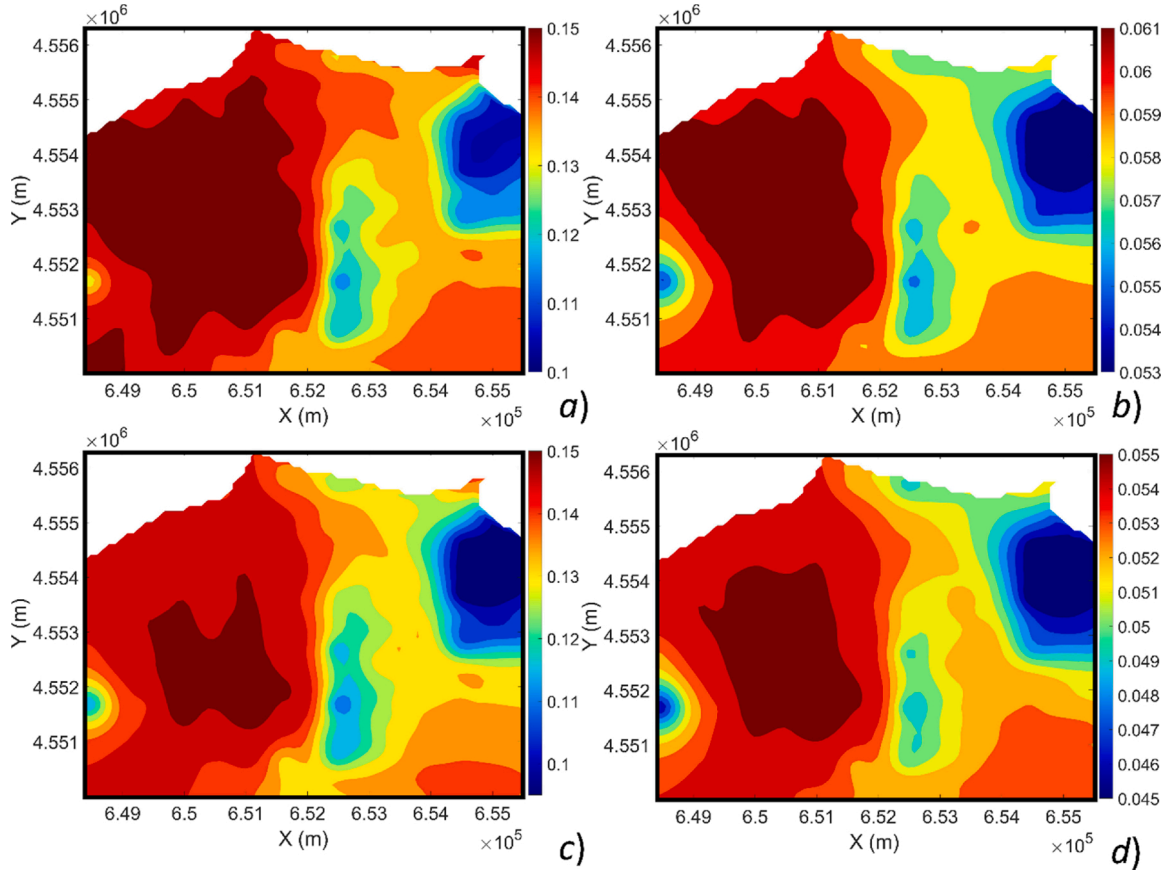

Fig. 12. Average thermal resistance distributions maps expressed in mKW^{-1} in heat recovery/dissipation mode. *a*) groundwater thermal resistance R_g in heat recovery mode ($T_p<T_0$) *b*) total borehole thermal resistance R_b+R_p in heat recovery mode with $R_p = 0.0139\ mKW^{-1}$ determined for a value of the mean pipe temperature of 283.15 K. *c*) groundwater thermal resistance R_g in heat dissipation mode ($T_p>T_0$). *d*) total borehole thermal resistance R_b+R_p in heat dissipation mode with $R_p = 0.0120\ mKW^{-1}$ determined for a value of the mean pipe temperature of 299.15 K.

fractured limestone aquifer by means of numerical simulations at local scale. It aims at illustrating the effect of respective aquifer parameter ranges on the field scale aiding a complementary field experiment. The fractured limestone aquifer of the Industrial area of Bari is used as a benchmark, but the proposed analysis is applicable to other sites with similar hydrogeological features. To investigate the heat transport processes, a three-dimensional flow and heat transport model corresponding of a section of 1 m of the gravel backfilled BHE surrounded by fracture limestone aquifer is set up.

Free convection flow is induced by temperature gradients that create density differences. The magnitude of free convective flow depends on the temperature differences between ambient groundwater temperature and mean water temperature into the heat exchanger. Heat exchanger modalities between BHE and aquifer are strictly dependent on the aquifer transmissivity. When aquifer transmissivity is minimum, the BHE works as a concentric cylindrical cavity with ascending (descending) free convective flow at the inner surface and descending (ascending) free convective flow at outer surface. Natural convective

flow increases heat transfer in BHE, whereas due to the lower value of the aquifer transmissivity heat transfer in the aquifer is governed mainly by heat conduction. As aquifer transmissivity increases, BHE and aquifer interact giving rise to the thermosyphon effect, free convection occurs in the aquifer further increasing the heat transfer. Heat advection due to groundwater flow is negligible until the groundwater Darcian velocity is lower than the critical value of 0.1 md^{-1}. In this last case advection mixes up with natural convection increasing the heat transfer processes. The advection contribution appears more relevant for a lower value of the temperature gradient, especially when the aquifers natural convection becomes negligible and the heat transfer processes is governed by advection.

The analysis of the BHE thermal resistance indicates that at lower groundwater flow heat transfer increases at least 25 % compared to pure heat conduction with stagnant water inside the BHE, reaching an increase from 140% to 300% when the aquifer transmissivity is maximum in the temperature interval of 278.15–304.15 K.

The outlined model represents a tool for predicting and quantifying BHE efficiency which may be used in TRT analysis and BHE design. The model would be a precursor of the thermal response test investigations in the field site in order to determine experimentally the advective and free convective influence in gravel back – filled borehole and validate the developed tool.

The obtained thermal resistance maps for the field site can help the design of a low enthalpy geothermal system that satisfies, in combination with other renewable technologies, the heat and cooling demand of the residential and industrial activities at the field site. The installation of several boreholes induces an interference effect among them which can reduce the BHEs efficiency. Darcian velocity and aquifer transmissivity represent the key parameters for optimizing the design of the borehole geothermal system. When aquifer transmissivity and Darcian velocity are low, the BHE interference is minimal and heat transfer in the aquifer is governed by heat conduction showing a great potential for seasonal heat storage. In the zones characterized by higher aquifer transmissivity and Darcian velocity, heat transfer in the aquifer is governed by advection with the implication that the plume of heat or coolth extends downgradient from the BHE, increasing the occurrence of the thermal interference. In this circumstance seasonal heat storage is not appropriate and the BHEs should work solely to recovery or dissipate heat for residential/industrial heating/cooling.

Due to the hydrogeological features, the aquifer at the field site presents a great potential for low enthalpy geothermal energy exploitation through the implementation of the gravel back – filled BHE system. However, groundwater contamination by chlorinated solvent together with seawater intrusion phenomena represent an environmental constraint for an extensive use of gravel back – filled BHE. As known, a permeable BHE creates a preferential pathway. Advection and density driven motion due to temperature differences permits mixing between shallow and deep groundwater and vice versa that could have a different grade of contamination. For this reason, gravel backfilled BHE should be no more than 30 m a.s.l deep, representing the mean boundary elevation of the shallow aquifer. Then BHE should be connected in series in order to obtain the working inlet – outlet temperature difference.

Authorship statement

All persons who meet authorship criteria are listed as authors, and all authors certify that they have participated sufficiently in the work to take public responsibility for the content, including participation in the concept, design, analysis, writing, or revision of the manuscript. Furthermore, each author certifies that this material or similar material has not been and will not be submitted to or published in any other publication before its appearance in the Geothermics.

CRediT authorship contribution statement

Nicola Pastore: Conceptualization, Methodology, Validation, Formal analysis, Investigation, Data curation, Writing - original draft, Writing - review & editing, Visualization. **Claudia Cherubini:** Validation, Investigation, Data curation, Writing - original draft, Writing - review & editing. **Concetta I. Giasi:** Validation, Investigation, Resources, Supervision, Funding acquisition.

Declaration of Competing Interest

The authors reported no declarations of interest.

Acknowledgements

The authors would like to acknowledge the two anonymous reviewers for their valuable comments and suggestions that helped improve the manuscript. This statement is signed by all the authors Author's name Author's signature Date Nicola Pastore 07 August 2020 Claudia Cherubini 07 August 2020 Concetta Immacolata Giasi 07 August 2020. This research was supported by Regional Authority under the program for groundwater remediation of polluted sites in the industrial area of Bari.

References

Alva, G., Lin, Y., Fang, G., 2018. An overview of thermal energy storage systems. Energy 144, 341–378. https://doi.org/10.1016/j.energy.2017.12.037.

Baietto, M., Pochettino, M., Salvatici, E., 2010. Progettazione di impianti geotermici. Sonde verticali e pozzi d'acqua, Dario Flaccovio Editore.

Baird, N., 2013. Geothermal conditioning: critical sources for sustainability. In: Loftness, V., Haase, D. (Eds.), Sustainable Built Environments. Springer New York, New York, NY, pp. 194–223. https://doi.org/10.1007/978-1-4614-5828-9_422.

Banks, D., 2015. A Review of the Importance of Regional Groundwater Advection for Ground Heat Exchange, pp. 2555–2565. https://doi.org/10.1007/s12665-014-3377-4.

Becker, M., Shapiro, A., 2000. Tracer transport in fractured crystalline rock: evidence of non diffusive breakthrough tailing. Water Resour. Res. 36, 1677–1686.

Beims, U., 1983. Planung, Dürchfuhrung und Auswertung von Gütepumpversuchen, Geohydrodynamische Erkundung. 25 -Z. angew. Geol 29 (10), 482–490. Berlin.

Billi, A., 2005. Attributes and influence on fluid flow of fractures in foreland carbonates of southern Italy. J. Struct. Geol. 27, 1630–1643.

Borgia, G.C., Bortolotti, V., Masciopinto, C., 2002. Valutazione del contributo della porosità effettiva alla trasmissività di acquiferi fratturati con tecniche di laboratorio e di campo. Ingegneria e Geologia degli Acquiferi, IGEA 17, 31–43.

Çengel, Y.A., Boles, M.A., 2001. Thermodynamics: an Engineering Approach. McGraw-Hill, Boston.

Cherubini, C., Pastore, N., Giasi, C.I., Allegretti, N.M., 2017. Laboratory experimental investigation of heat transport in fractured media. Nonlinear Process. Geophys. 24, 23–42. https://doi.org/10.5194/npg-24-23-2017.

Cherubini, C., Pastore, N., Rapti, D., Giasi, C.I., 2018. Numerical modeling of flow and transport in the Bari industrial areaby means of rough walled parallel plate and random walk models. Hydrol. Earth Syst. Sci. Discuss. 22, 5211–5225. https://doi.org/10.5194/hess-22-5211-2018, 2018.

Chiasson, A., Rees, S.J., Spitler, J.D., 2000. A preliminary assessment of the effects of ground-water flow on closed-loop ground-source heat pump systems. ASHRAE Trans. 106 (1), 380–393.

Choi, W., Ooka, R., 2016. Effect of natural convection on thermal response test conducted in saturated porous formation : comparison of gravel-back filled and cement-grouted borehole heat exchangers. Renew. Energy 96, 891–903. https://doi.org/10.1016/j.renene.2016.05.040.

Churchill, S.W., 1977. Friction factor equations spans all fluid-flow regimes. Chem. Eng. J. 84, 91–92.

Claesson, J., Hellström, G., 2000. Analytical studies of the influence of regional groundwater flow on the performance of borehole heat exchangers. In: Terrastock 8th International Conference on Thermal Energy Storage. Stuttgart, Germany.

Di Sipio, E., Galgaro, A., Destro, E., Giaretta, A., Chiesa, S., VIGOR Team, 2016. Thermal conductivity of rocks and regional mapping. In: European Geothermal Congress Pisa. Italy 3–7 June 2013.

Ehyaei, M.A., Ahmadi, A., Haj, El, Assad, M., Rosen, M.A., 2020. Investigation of an integrated system combining an Organic Rankine Cycle and absorption chiller driven by geothermal energy: energy, exergy, and economic analyses and optimization. J. Clean. Prod. 258, 120780 https://doi.org/10.1016/j.jclepro.2020.120780.

Ergun, S., 1953. Fluid flow through packed columns. Chem. Eng. Prog. 48, 89–94.

Fujii, H., Okubo, H., Nishi, K., Itoi, R., Ohyama, K., Shibata, K., 2009. An improved thermal response test for U-tube ground heat exchanger based on optical fiber thermometers. Geothermics 38, 399–406. https://doi.org/10.1016/j.geothermics.2009.06.002.

Gehlin, S., Hellström, G., 2003. Influence on thermal response test by groundwater flow in vertical fractures in hard rock. Renew. Energy 28, 2221–2238.
Gehlin, S., Hellström, G., Nordell, B., 2003. The influence of the thermosiphon effect on the thermal response test. Renew. Energy 28, 2239–2254.
Gnielinski, V., 1976. New equations for heat and mass transfer in turbulent pipe and channel flow. Int. Chem. Eng. 16 (2), 359–368, 1976.
Grassi, D., Sdao, F., Tadolini, T., 1986. Idrogeologia dell'area posta a cavallo della Murgia e del Tavoliere di Puglia. Geol. Appl. e Idro. XXI, 85–98.
Gustafsson, A.-M., Westerlund, L., 2010. Multi-injection rate thermal response test in groundwater filled borehole heat exchanger. Renew. Energy 35, 1061–1070. https://doi.org/10.1016/j.renene.2009.09.012.
Gustafsson, A., Westerlund, L., Hellström, G., 2010. CFD – modelling of natural convection in a groundwater-filled borehole heat exchanger. Appl. Therm. Eng. 30 (6–7), 683–691. https://doi.org/10.1016/j.applthermaleng.2009.11.016.
Handley, D., Heggs, P., 1968. Momentum and heat transfer mechanisms in regular shaped packings. Trans. Am. Inst. Chem. Eng. 46 (9), 251–259.
Heiko, T.L., Javed, S., Vistness, G., 2012. Multi – injection rate thermal response test with forced convection in a groundwater-filled borehole in hard rock. Renew. Energy 48, 263–268.
Heinze, T., Hamidi, S., 2017. Heat transfer and parameterization in local thermal non-equilibrium for dual porosity continua. Appl. Therm. Eng. 114, 645–652. https://doi.org/10.1016/j.applthermaleng.2016.12.015.
Hidalgo, J.J., Carrera, J., Dentz, M., 2009. Steady state heat transport in 3D heterogeneous porous media. Adv. Water Resour. 32, 1206–1212. https://doi.org/10.1016/j.advwatres.2009.04.003.
Kambiz, V., 2005. Handbook of Porous Media. CRC Press Taylor & Francis Group, Boca Raton FL.
Keyhani, M., Kulacki, F., Christensen, R.N., 1983. Free Convection in a Vertical Annulus With Constant Heat Flux on the Inner Wall. (August). https://doi.org/10.1115/1.3245606.
Klepikova, M.V., Le Borgne, T., Bour, O., Dentz, M., Hochreutener, R., Lavenant, N., 2016. Heat as a tracer for understanding transport processes in fractured media: theory and field assessment from multiscale thermal push-pull tracer tests. Water Resour. Res. 52, 5442–5457. https://doi.org/10.1002/2016WR018789.
Lallemand-Barres, A., Peaudecerf, P., 1978. Recherche des *relations entre* la *valeur* de la *dispersivité macroscopique* d'un *milieu aquifere, ses autres caractéristiques* et les *conditions* de mesure. Bull. Bur. Rech. Geol. Minières (Fr.) Sect. 3 (4), 277.
Laskowski, G.M., Kearney, S.P., Evans, G., Greif, R., 2007. Mixed convection heat transfer to and from a horizontal cylinder in cross-flow with heating from below. Int. J. Heat Fluid Flow 28, 454–468. https://doi.org/10.1016/j.ijheatfluidflow.2006.05.004.
Luo, J., Tuo, J., Huang, W., Zhu, Y., Jiao, Y., Xiang, W., Rohn, J., 2018. Influence of groundwater levels on effective thermal conductivity of the ground and heat transfer rate of borehole heat exchangers. Appl. Therm. Eng. 128, 508–516. https://doi.org/10.1016/j.applthermaleng.2017.08.148.
Masciopinto, C., Palmiotta, D., 2016. A new method to infer advancement of saline front in coastal groundwater systems by 3D: the case of bari (Southern Italy) fractured aquifer. Computation 4, 9. https://doi.org/10.3390/computation4010009.
Minchio, F., Cesari, G., Pastore, C., Fossa, M., 2020. Experimental hydration temperature increase in borehole heat exchangers during thermal response tests for geothermal heat pump design. Energies 13, 3461. https://doi.org/10.3390/en13133461.
Molina-Giraldo, N., Blum, P., Zhu, K., Bayer, P., Fang, Z., 2011. A moving finite line source model to simulate borehole heat exchangers with groundwater advection. Int. J. Therm. Sci. 50, 2506–2513. https://doi.org/10.1016/j.ijthermalsci.2011.06.012.
Nazridoust, K., Ahmadi, G., Smith, D.H., 2006. A new friction factor correlation for laminar, single-phase flows through rock fractures. J. Hydrol. 329, 315–328.
Ouyang, X.L., Xu, R.N., Jiang, P.X., 2017. Three-equation local thermal non-equilibrium model for transient heat transfer in porous media: the internal thermal conduction effect in the solid phase. Int. J. Heat Mass Transf. 115, 1113–1124. https://doi.org/10.1016/j.ijheatmasstransfer.2017.07.088.
Ozgener, O., 2010. Use of solar assisted geothermal heat pump and small wind turbine systems for heating agricultural and residential buildings. Energy 35, 262–268. https://doi.org/10.1016/j.energy.2009.09.018.
Pastore, N., Cherubini, C., Rapti, D., Giasi, C.I., 2018. Experimental study of forced convection heat transport in porous media. Nonlinear Process. Geophys. Discuss. 25, 279–290.
Pastore, N., Cherubini, C., Giasi, C.I., Rapti, D., 2020. Numerical model of the behavior of chlorinated ethenes in a fractured, karstic limestone aquifer. Hydrogeol. J. https://doi.org/10.1007/s10040-020-02248-1.
Poulsen, S.E., Alberdi-Pagola, M., 2015. Interpretation of ongoing thermal response tests of vertical (BHE) borehole heat exchangers with predictive uncertainty based stopping criterion. Energy 88, 157–167. https://doi.org/10.1016/j.energy.2015.03.133.
Pruess, K., 2010. Thermal Single-well Injection-Withdrawal Tracer Tests for Determining Fracture-Matrix Heat Transfer Area. Lawrence Berkeley Natl. Lab.
Read, T., Bour, O., Bense, V., Le Borgne, T., Goderniaux, P., Klepikova, M.V., Hochreutener, R., Lavenant, N., Boschero, V., 2013. Characterizing groundwater flow and heat transport in fractured rock using fiber-optic distributed temperature sensing. Geophys. Res. Lett. 40, 2055–2059. https://doi.org/10.1002/grl.50397.
Robertson, E.C., 1988. Thermal Properties of Rocks. US Department of the Interior: Geological Survey, pp. 88–441.
Roux, S., Plouraboué, F., Hulin, J.P., 1998. Tracer dispersion in rough open cracks. Transp. Porous Media 32, 97–116.
Samuel, D.G.L., Nagendra, S.M.S., Maiya, M.P., 2013. Passive alternatives to mechanical air conditioning of building: a review. Build. Environ. 66, 54–64. https://doi.org/10.1016/j.buildenv.2013.04.016.
Self, S.J., Reddy, B.V., Rosen, M.A., 2013. Geothermal heat pump systems: status review and comparison with other heating options. Appl. Energy 101, 341–348. https://doi.org/10.1016/j.apenergy.2012.01.048.
Shah, S.K., Aye, L., Rismanchi, B., 2018. Seasonal thermal energy storage system for cold climate zones: a review of recent developments. Renew. Sustain. Energy Rev. 97, 38–49. https://doi.org/10.1016/j.rser.2018.08.025.
Skarphagen, H., Banks, D., Frengstad, B.S., Gether, H., 2019. Design considerations for borehole thermal energy storage (BTES): a review with emphasis on convective heat transfer. Geofluids 2019, 4961781. https://doi.org/10.1155/2019/4961781.
Spitler, J.D., Gehlin, S.E.A., 2015. Thermal response testing for ground source heat pump systems—an historical review. Renew. Sustain. Energy Rev. 50, 1125–1137. https://doi.org/10.1016/j.rser.2015.05.061.
Spitler, J.D., Javed, S., Kalskin, R., 2016. Natural convection in groundwater-filled boreholes used as ground heat exchangers. Appl. Energy 164, 352–365. https://doi.org/10.1016/j.apenergy.2015.11.041.
Stuke, B., 1948. Berechnung des Wärmeaustausches in Regeneratoren mitzylindrischem und kugelförmigem Füllmaterial. Angew. Chem. 20 (10), 262–268.
Trillat-Berdal, V., Souyri, B., Achard, G., 2007. Coupling of geothermal heat pumps with thermal solar collectors. Appl. Therm. Eng. 27, 1750–1755. https://doi.org/10.1016/j.applthermaleng.2006.07.022.
Verdoya, M., Chiozzi, P., 2015. Influence of groundwater flow on the estimation of subsurface thermal parameters. Int. J. Earth Sci. https://doi.org/10.1007/s00531-016-1397-x. September 2017.
Wagner, R., Clauser, C., 2005. Evaluating thermal response tests using parameter estimation for thermal conductivity and thermal capacity. J. Geophys. Eng. 2, 349–356. https://doi.org/10.1088/1742-2132/2/4/S08.
Wagner, V., Blum, P., Kübert, M., Bayer, P., 2013. Analytical approach to groundwater-influenced thermal response tests of grouted borehole heat exchangers. Geothermics 46, 22–31. https://doi.org/10.1016/j.geothermics.2012.10.005.
Williams, M.D., Newell, D., Watson, T., Vermeul, V.R., Reimus, P.W., Pacific Northwest National Laboratory, 2010. Development of Models to Simulate Tracer Behavior in Enhanced Geothermal Systems. Prep. U. S. Dep. Energy Under Contract DE-AC05-76RL01830 44.
Witte, H.J.L., 2001. Geothermal response test with heat extraction and heat injection: examples of application in research and design of geothermal heat exchangers. Workshop Lausanne. October 2001.
Witte, H.J.L., 2013. Error analysis of thermal response tests. Appl. Energy 109, 302–311. https://doi.org/10.1016/j.apenergy.2012.11.060.
Wu, X., Pope, G.A., Shook, G.M., Srinivasan, S., 2008. Prediction of enthalpy production from fractured geothermal reservoirs using partitioning tracers. Int. J. Heat Mass Transf. 51, 1453–1466. https://doi.org/10.1016/j.ijheatmasstransfer.2007.06.023.
Xu, J., Wang, R.Z., Li, Y., 2014. A review of available technologies for seasonal thermal energy storage. Sol. Energy 103, 610–638. https://doi.org/10.1016/j.solener.2013.06.006.
Yilmaz, C., 2017. Thermodynamic and economic investigation of geothermal powered absorption cooling system for buildings. Geothermics 70, 239–248. https://doi.org/10.1016/j.geothermics.2017.06.009.
Zeiler, W., Boxem, G., 2009. Geothermal active building concept. In: Howlett, R.J., Jain, L.C., Lee, S.H. (Eds.), Sustainability in Energy and Buildings. Springer, Berlin Heidelberg, Berlin, Heidelberg, pp. 305–314.
Zeng, H.Y., Diao, N.R., Fang, Z.H., 2002. A finite line-source model for boreholes in geothermal heat exchangers. Heat Transf. - Asian Res. 31, 558–567. https://doi.org/10.1002/htj.10057.